Pitch angle control with fault diagnosis and tolerance for wind turbine generation systems

Yiran Shi[1], Shoutao Li[1], Shuangxin Wang[2], Yujia Zhai[3], Yantao Tian[1], Ding-Li Yu[4,1,$]

[1] Faculty of Communication Engineering, Jilin University, Changchun, China.
[2] School of Mechanical and Control Engineering, Beijing Jiaotong University, Beijing, China.
[3] Department of Electrical and Electronic Engineering, Xian Jiao Tong Liverpool University, Suzhou, Jiangsu, China.
[4] Control Systems Research Group, Liverpool John Moores University, Byrom Street, Liverpool L3 3AF, U.K.
[$] Corresponding author: D.Yu@ljmu.ac.uk

Abstract. To enhance the reliability of wind turbine generation systems that are generally located in the remote area and subjected to harsh environment, we design the pitch angle control for variable-speed wind turbines with function of fault diagnosis and fault tolerance. The main fault targeted in this research is the mechanical wear and possible break of the blade, pitch gear set or shaft, which cause shaft rotary friction change. The proposed method uses a disturbance observer to diagnose the fault. The estimated fault is used for component assessment and later maintenance. The fault tolerant control is achieved using a full-order terminal sliding mode control combined with an adaptive neural network estimator. With the compensation of the adaptive estimator, the post fault states can be driven onto the sliding surface and converge to a small area around the origin. The full-order terminal sliding mode control ensures the state convergence in finite time. The Lyapunov method is used to derive the control law so that the closed-loop post fault stability and the convergence of the adaptive estimator adaptation are both guaranteed. The computer simulations of the pitch angle control based on a 5-MW variable- speed variable-pitch angle wind turbine model are conducted with different types of fault simulated. A third-order nonlinear state space model with fault term is derived, and real physical parameters are applied in the simulations. The simulation results demonstrate the feasibility and effectiveness of the proposed scheme and potential of real world applications.

Keywords. Pitch angle control, variable speed wind turbines, fault tolerant control, **t**erminal sliding mode, adaptive neural networks.

1. Introduction

Wind turbine generation systems have been recognised in the past decades as most productive green energy source and are witnessed rapid growth. To cope with the frequent change of wind speed in a big range, the variable speed wind turbines (VSWT) have shown their advantages and therefore are adopted, see the current status on VSWT from a survey paper [1]. In the wind turbine management schemes wind speed is divided into three regions, and the

variable speed wind turbines work in different modes when the wind speed falls in different regions. When the wind speed is higher than the rated speed that is referred to region 3 and matches the maximal generation power, the power output of a VSWT will be maintained at the rated power to avoid large aerodynamic force to be generated through blades, which leads to over-speeding of generator rotor and causes generator overheat. Furthermore, maintaining the rated speed can also cope with the fluctuation of the wind speed, such as gusts, which will cause large turbine load and may lead to component fatigue, automatic shutdown or even damage some components of the turbine. There have been a great deal of research on management of VSWT, such as a new structure of sliding mode control [2], a fault detection and monitoring scheme for the VSWT [3], and a control approach using a robust wind torque estimation [4], etc.

A basic method to cope with high wind speed is to change the conversion rate of wind dynamic energy to the energy captured by the wind turbine blades, which can be achieved by adjusting the blade pitch angle. Generally, there are two types of pitch operation systems. One is the electro-mechanical system that employs an electrical servomotor to drive pitch turbine blades. The other is the hydraulic pitch system, which uses a servo valve-controlled hydraulic cylinder to drive the blades through a slider-crank mechanism, to convert the linear displacement of the cylinder to the pitch angle of the blades. The electro-mechanical pitch system suffers from limited torque and low power to mass ratio; while the hydraulic pitch system suffers from low accuracy of hydraulic systems. In this research we consider an electro-hydraulic servo pitch system, which employs a hydraulic pump controlled hydraulic motor to manipulate the pitch angle.

There exist some pitch angle control schemes in the literature. Linear control techniques were used in the early stage. For example, the three-term (PID) regulator was implemented in [5, 6] to compensate for nonlinear aerodynamic at different wind speeds. The linear control has a drawback that while the control parameters were tuned for one operating point, the control performance would be degraded when the wind turbine worked away from the operating point. The gain scheduling technique was also investigated [7, 8], where adaptation of control parameters still relied on the measurement of wind speed. The optimal control with linear quadratic cost function was attempted in [9]. While it could provide steady output power, the method is linear and the implementation needs linearization.

As the dynamics of hydraulic pumps, motors and flow through valves are all nonlinear, some intelligent control techniques have been applied. A hydraulic pitch system driven by two differential hydraulic cylinders was developed in [10]. An adaptive fuzzy controller with self-tuning fuzzy sliding mode compensation was used to control the developed system. However, the pitch rate limitation was not fully eliminated, the desired control performances has an offset. A pitch controller was designed in [11] to smooth output fluctuations at different wind speeds. [12] developed a pitch angle control using a fuzzy controller with the generator output power and rotor speed as the two inputs. Neural networks also found applications in pitch angle control systems. The pitch angle controller designed in [13, 14] used the radial basis function (RBF) network for different operation modes. The RBF network used in [15]

was trained with the back-propagation algorithm and regulated the wind power capture.

Nonlinear control strategy has also been applied to the pitch angle control for power regulation at different wind speeds. For example, the feedback linearization was used in [16] to cancel turbine nonlinearities. A nonlinear proportional plus integral (PI) control was proposed in [17] for pitch angle with an extended state estimator to compensate for unknown time-varying nonlinearities. In [18] a nonlinear robust scheme was developed for wind turbine output control. Sliding-mode approaches were utilized in [19-21] to design the pitch angle system, but their chattering has not been eliminated.

Fault detection and fault tolerant control has been approved to be effective in enhancing the reliability of more and more complex control systems in modern industry. Fault detection aims at reporting fault occurrence within a control system due to component or sensor malfunction and is used to schedule maintenance and repair. Fault tolerant control is to stabilize the post-fault dynamics and maintain control performances until the fault is fixed. Some methods have been developed recently, such as [22] using adaptive neural networks, [23] using back-stepping technique, and [24] using integral SMC. [25, 26] used RBF network as on-line estimator for fault detection, and [27, 28] applied these estimators to estimate unknown parameters in automotive engine control, and tune sliding mode gain, to achieve robust regulation against disturbance. [29] developed an improved sliding mode control scheme with time-delay estimation for motion tracking control. However, the sliding mode method is often subject to two major problems when it is applied to industrial systems: one is that the singularity in the closed-loop system and the other is that the state chattering around the selected sliding manifold. Therefore, developing a special type of sliding mode control strategy to overcome the specified two shortcomings and with effective robust performance against disturbance and system fault is currently a very challenging task.

As the nominal sliding mode control can reject matched disturbance only and may not guarantee finite time convergence [30], a terminal sliding mode control (TSMC) was proposed with some superior features, such as finite-time convergence and robustness to matched uncertainty [31-32]. However, the TSMC may suffer two problems: one is the singularity in the design and the other is the output chattering. If a negative fractional power exists in the control variable, singularity will occur, which will cause the control variable unbounded. Chattering causes control variable oscillation across the sliding manifold, which will cause mechanical wear of the actuators. To avoid these drawbacks researchers in [33-34] tackled the problems to improve the convergence property. However, as they used the reduced-order TSMC, the state away the sliding surface achieves finite-time convergence to a bounded layer around zero, instead of origin, so that the characteristics lost. To achieve a finite-time convergence to the origin, a novel concept of full-order TSMC (FOTSMC) was proposed in [35], which overcome the two problems of singularity and chattering. However, this full order TSMC requires that the bounds of derivative of system disturbance must be known for its application. This greatly limits its applications in real world, as the bounds of derivative may not be known in practice. Therefore, this limitation needs to be got rid of to gain wider industrial applications.

In this paper, an AC servo motor-driven hydraulic pump is used to drive a hydraulic motor, and the hydraulic motor drives the blades through a gear set to implement pitch angle control. A nonlinear dynamic model of the hydraulic system is derived. In the model the nonlinear dynamics of the viscous and coulomb frictions of the hydraulic motor, gear set and blades are considered to be a major fault of the system, as these frictions have often a significant change in practice to prevent the system from normal operation. The friction changes will cause a significant load torque change for the pitch angle drive system. To achieve the tracking of the real pitch angle to the desired pitch angle and tolerance to the fault stated above, we developed a FOTSMC scheme in this work for the hydraulic pitch angle drive system, and combine the control scheme with a disturbance observer to achieve the fault detection and fault tolerant control. An adaptive RBF network is used to estimate the change rate of the fault in the FOTSMC scheme; the bounds of the change rate of the fault as the limitation to the method in [35] are relaxed

The novelty and major contributions of this paper are as follows: (a) The upper bound of change rate of the fault considered is not required in the developed RBF estimator associated FOTSMC. (b) Friction change that often occurs in the real world wind turbine generation systems is tolerated as the fault whilst the pitch angle tracking control is achieved. (c) Post-fault stability of the closed-loop system and the convergence of the adaptive RBF network estimator are guaranteed with Lyapunov theory. (d) The developed new control strategy is applied to a hydraulic pitch angle drive control system and achieves pitch angle tracking control with friction fault detection and tolerance.

The paper is organised as follows. The modelling of the hydraulic actuator system and the fault presentation is described in Section 2. Section 3 presents the disturbance observer and fault detection. The developed fault tolerant control scheme using the FOTSMC and adaptive RBF estimator is presented in Section 4. Application of the developed method to the hydraulic pitch angle control system is evaluated by computer simulations, which is described in Section 5. To emphasize the advantage of the proposed method, a comparative study is given in Section 6. Finally, some conclusions are drawn in Section 7.

2. Hydraulic pitch system modelling

The pitch drive actuator system studied in this research includes a variable speed hydraulic pump that integrates an AC servomotor with an axial piston pump. The rotor of the servomotor is rigidly coupled to the barrel of the pump [36]. The pump is used to drive a hydraulic motor, and the motor is to convert high-speed low-torque power to low-speed high-torque power through a gear set to drive the high load torque of blades. The schematic of the hydraulic pitch drive system is shown in Fig.1.

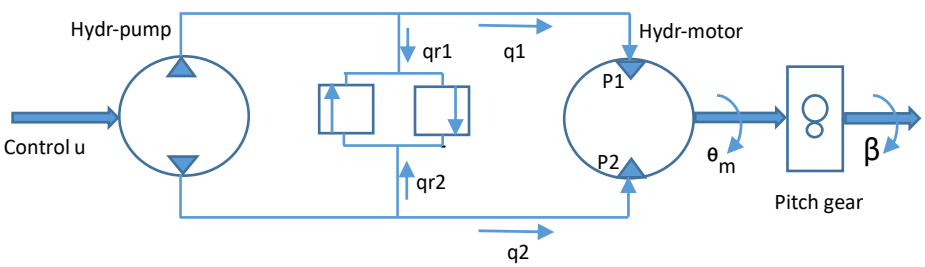

Fig.1 Schematic of pitch angle drive system

It can be seen in the above system that the manipulated variable is the voltage signal of the servomotor input, while the variable to be controlled is the pitch angle of the blades. It is a servo control with the desired blade pitch angle (reference signal) generated by the wind turbine power control system according to the variable wind speed. Therefore, the pitch angle control system designed here is a subsystem of the total wind turbine power control system.

The control signal input to the AC servomotor is transferred to the rotary speed of the hydraulic motor. As the servo motor dynamics has much faster response than that of the hydraulic components in the system, the servo motor dynamics is neglected for simplicity and the only the static gain remains.

$$\omega_p(t) = K_a u(t) \tag{1}$$

where ω_p is the rotary speed of the servo motor and K_a is the gain of the servo control unit. The flow dynamics in the inlet pipe and outlet pipe of the hydraulic pump are described by the following two equations respectively.

$$q_1(t) = D_p\omega_p(t) - C_{tp}[P_1(t) - P_2(t)] - q_{r1}(t) \tag{2}$$

$$q_2(t) = D_p\omega_p(t) - C_{tp}[P_1(t) - P_2(t)] - q_{r2}(t) \tag{3}$$

where q_1, q_2 are the hydraulic flow rates, D_p the volumetric displacement of the pump, P_1, P_2 the chamber pressures of the hydraulic motor, C_{tp} are the leakage coefficient of the pump, respectively. q_{r1}, q_{r2} denote the flow rates through the two relief valves respectively, which have been set to zero considering that the chamber pressure of the hydraulic motor is always lower than the pre-set pressure of the relief valve under normal operating conditions. On the other hand, the continuity equations of the hydraulic dynamics at the motor side of the motor chamber are,

$$q_1(t) = D_m\omega_m(t) + C_{tm}[P_1(t) - P_2(t)] + \frac{V_1 + D_m\theta_m(t)}{\beta_e}\dot{P}_1(t) \tag{4}$$

$$q_2(t) + \frac{V_2 - D_m\theta_m(t)}{\beta_e}\dot{P}_2(t) = D_p\omega_m(t) - C_{tm}[P_1(t) - P_2(t)] \tag{5}$$

Where V_1, V_2 are the original total control volumes of the hydraulic motor chambers respectively, and β_e is the effective bulk modulus of the hydraulic fluid,. The others are the counterparts of the motor corresponding to that of the pump.

The torque balance equation of the hydraulic motor is derived as,

$$D_m[P_1(t) - P_2(t)] = J_t\ddot{\theta}_m(t) + G\theta_m(t) + T_p(t) \tag{6}$$

where J_t denotes the total inertia of the hydraulic motor and G is the pitch load spring gradient. $T_p(t)$ in (6) represents the load torque including the active torque need to drive the blades, which is converted through the pitch gear, and resistant torque generated by friction increment on the hydraulic motor axis, which is treated as fault in this study. Finally, the resulting pitch angle of the gear set output is given by,

$$\beta(t) = \frac{\theta_m(t)}{i_g} \tag{7}$$

where β and i_g denote the pitch angle and gear ratio respectively.

The dynamics of servo motor-hydraulic drive presented in equation (1)-(7) are concluded as a third-order derivative of hydraulic motor shaft angle with respect to time.

$$\dddot{\theta}_m = \frac{1}{J_t}[D_m(\dot{P}_1 - \dot{P}_2) - G\ddot{\theta}_m - \dot{T}_p]$$

$$= \frac{D_m}{J_t}\begin{Bmatrix} \frac{\beta_e}{V_1 + D_m\theta_m}\left[D_p\omega_p - D_m\omega_m - (C_{tp} + C_{tm})(P_1 - P_2)\right] \\ -\frac{\beta_e}{V_2 - D_m\theta_m}\left[D_p\omega_m - D_p\omega_p + (C_{tp} - C_{tm})(P_1 - P_2)\right] \end{Bmatrix} - \frac{1}{J_t}(G\ddot{\theta}_m - \dot{T}_p) \tag{8}$$

A third-order state space model is set up using the dynamics in (8) by selecting three states: $x_1 = \beta(t),\ x_2 = \dot{\beta}(t),\ x_3 = \ddot{\beta}(t)$.

$$\dot{x}_1 = x_2$$

$$\dot{x}_2 = x_3$$

$$\dot{x}_3 = \frac{D_m\beta_e}{J_t(V_1 + D_m i_g x_1)}\left[-D_m x_2 - \frac{C_{tp} + C_{tm}}{D_m}\left(J_t x_3 + G x_1 + \frac{T_p(t)}{i_g}\right) + \frac{D_p K_a}{i_g}u(t)\right]$$

(9)

$$-\frac{D_m\beta_e}{J_t(V_2 - D_m i_g x_1)}\left[D_p x_2 + \frac{C_{tp} - C_{tm}}{D_m}\left(J_t x_3 + G x_1 + \frac{T_p(t)}{i_g}\right) - \frac{D_p K_a}{i_g}u(t)\right] - \frac{G}{J_t}x_3 - \frac{\dot{T}_p(t)}{J_t i_g}$$

where C_{tp}, C_{tm} are leakage coefficients of the hydraulic pump and motor respectively.

Equation (9) is of a general form as follows,

$$\dot{x}_3 = g(x) + b(x)u(t) + f(t)$$

(10)

with $g(x) = -\frac{D_m\beta_e}{J_t}\{\frac{1}{V_1+D_m i_g x_1}[D_m x_2 + \frac{C_{tp}+C_{tm}}{D_m}(J_t x_3 + G x_1)]$

$$+\frac{1}{V_2-D_m i_g x_1}[D_m x_2 + \frac{C_{tp}+C_{tm}}{D_m}(J_t x_3 + G x_1)]\} - \frac{G}{J_t}x_3 \quad (11)$$

$$b(x) = \frac{D_m\beta_e D_p K_a}{J_t i_g}\left(\frac{1}{V_1+D_m i_g x_1} + \frac{1}{V_2-D_m i_g x_1}\right) \quad (12)$$

$$f(t) = -\frac{\beta_e(C_{tp}+C_{tm})}{J_t i_g} * \frac{1}{V_1+D_m i_g x_1} * T_p(t) - \frac{1}{J_t i_g}\dot{T}_p(t) \quad (13)$$

Here, $f(t)$ denotes the fault signal to be detected and tolerant in the designed control system. In this research $f(t)$ is a function of $T_p(t)$ and derivative of $T_p(t)$, with $T_p(t)$ the added viscous and column friction of pitch system axis and gear set, which is caused by a frequently occurred component failure in a wind turbine generation system. This completes the modelling. All variables and physical parameters in the model are listed in Table 1.

Table 1 Variables and physical parameters in the model

Variables	Definition (Units)
$u(t)$	Servo motor control (V)
$\omega_p(t)$	Rotary speed of the servo motor (rad/sec)
$q_1(t)$	Inlet flow rate of hydraulic pump (m^3/sec)
$q_2(t)$	Outlet flow rate of hydraulic pump (m^3/sec)
$P_1(t)$	Chamber pressure of hydraulic motor in high pressure side (Pa)
$P_2(t)$	Chamber pressure of the hydraulic motor in low pressure side (Pa)
$q_{r1}(t)$	Flow rate through inlet relieve valve (m^3/sec)
$q_{r2}(t)$	Flow rate through outlet relieve valve (m^3/sec)
$\omega_m(t)$	rotary speed of the hydraulic motor (rad/sec)
$\theta_m(t)$	Rotary displacement of hydraulic motor (rad)
$f(t)$	Load torque on the motor shaft (Nm)
$\beta(t)$	Pitch angle (rad)
$T_p(t)$	Added viscous and column friction of pitch system axis and gear set caused by occurred component failure
Parameters	**Definition (Units)**
K_a	Gain of the servo motor unit (rad/s/V) 0.5
D_p	Volumetric displacement of the pump (m^3/rad) 0.03
C_{tp}	Leakage coefficient of the pump (m^3/s/Pa) $0.5*10^{-11}$
β_e	Bulk modulus of the hydraulic fluid (Pa) $2.0*10^9$ Pa
V_1	Original total control volume of hydraulic motor chamber in the high pressure side (m^3) $0.01m^3$
V_2	Original total control volume of hydraulic motor chamber in the low pressure side (m^3) $0.04m^3$
D_m	Volumetric displacement of the motor (m^3/rad) 0.002
C_{tm}	Leakage coefficient of the motor (m^3/s/Pa) $0.6*10^{-11}$
J_t	Total inertia of hydraulic motor (kgm^2) 138
G	Pitch load spring gradient (kgm^2s^2) 0.1
i_g	Pitch angle gear ratio 30

3. Disturbance observer and fault detection

We develop, in this work, a disturbance observer for fault detection purpose and for assisting the fault tolerant control of the variable speed pitch angle system. For system model in (10) and (12), we present the model in the following vector-matrix form.

$$\dot{x} = g_1(x) + g_2(x)u(t) + Hf(t) \tag{14}$$

with $x = [x_1 \ x_2 \ x_3]^T \in R^3$, $g_1(x) = [x_2 \quad x_3 \quad g(x)]^T$, $g_2(x) = [0 \quad 0 \quad b(x)]^T$, $H = [0 \quad 0 \quad 1]^T$. Here, x is the system state vector, $u \in R$ is the system input, $g(x)$ in g_1 and $b(x)$ in g_2 are smooth and continuous nonlinear functions with $g(0) = 0$ and $b(x) \neq 0$.

$f(t)$ is an unknown time function representing the system fault.

Assumption

The fault signal in (14), $f(x)$ bounded:

$$|f(x)| \leq B_f$$

where B_f is constant. This assumption is reasonable and is generally satisfied in engineering problems.

A disturbance observer for system (14) is designed as follows.

$$\begin{cases} \dot{z} = -PHz - P[HPx + g_1(x) + g_2(x)u] \\ \hat{f} = z + Px \end{cases} \tag{15}$$

where $z \in R$ is the internal state variable, $P \in R^{1\times 3}$ is the observer gain matrix, and $\hat{f}$ is the observer output, the estimate of the fault.

Let us analyse the stability and performance of the disturbance observer. For fault estimation error defined as, $e_f = f - \hat{f}$, we have its dynamics,

$$\dot{e}_f = \dot{f} - \dot{\hat{f}} = \dot{f} - \dot{z} - P\dot{x} = \dot{f} + PHz + PHPx - PHf$$

$$= \dot{f} - PHe_f$$

This leads to

$$\dot{e}_f + PHe_f = \dot{f} \tag{16}$$

It is obvious that if P is designed such that $PH>0$, (16) will be stable. Furthermore, if the fault is a constant signal, the fault estimation error will converge to zero, i.e. the fault estimation in the steady state is accurate. However, this is often not the case in the industrial applications as some faults are time varying. With further analysis, it can be seen that the real fault is related to the estimated fault by the following equation. It can be derived from (15),

$$\dot{\hat{f}} = PHe_f = PHf - PH\hat{f} \tag{17}$$

Then, it is concluded that the estimated fault is a low-pass first-order filter output of original fault signal, and the time constant of the filter is $\tau = PH$. Although estimated fault cannot be used as the real fault, it is reasonable to use the estimated fault as a fault detection signal to report the occurrence of the fault. Furthermore, the fault estimation error can be reduced if P is designed small. This feature of the estimated fault is clearly illustrated by the simulation studies in Section 5. Such a disturbance observer is used for fault detection purpose for the pitch angle control system and the performance is demonstrated in the simulations in Section 5.

4. Fault tolerant control scheme

The objective of the fault tolerant control scheme in this paper is to design a control system for the nonlinear system in (10) and (12) so that the output x_1 tracks the reference signal, and when a fault occur the closed-loop system is guaranteed stable with the tracking performance not influenced by the fault. To achieve this objective, we designed a full-order terminal sliding mode control with a RBF network on-line updated to compensate the effects of the occurring fault.

For an n^{th} order nonlinear system with a model in (18), we develop a full-order terminal sliding mode control in conjunction to an adaptive RBF network estimator to achieve the convergence of system state in finite time. The developed control scheme is then applied to the variable speed wind turbine generation systems to achieve pitch angle fault tolerant tracking control.

$$\begin{cases} \dot{x}_1 = x_2 \\ \dot{x}_2 = x_3 \\ \vdots \\ \dot{x}_{n-1} = x_n \\ \dot{x}_n = g(x) + f(x) + b(x)u \end{cases} \tag{18}$$

where $x = [x_1 \ \cdots \ x_n]^T \in R^n$ is the system state, $u \in R$ is system input, $g(x)$ and $b(x)$ are smooth continuous nonlinear functions with $g(0) = 0$ and $b(x) \neq 0$. In equation (18), $f(x)$ denotes the fault signal in the system. The fault is unknown a continuous time function and is bounded. Moreover, the first-order derivative of the fault is also a continuous function and is bounded. The bound of the fault change rate does not need to be known. This assumption is reasonable and is generally satisfied in engineering problems.

Definition

A definition similar to that in [35] is used here for a FOTSM manifold, but the tracking error rather than system state is used for reference tracking control.

$$s = \dot{e}_n + \beta_n e_n^{\alpha_n} + \cdots + \beta_1 e_1^{\alpha_1} \tag{19}$$

Where $e_i \ (i = 1, \cdots, n)$ is the tracking error defined as below with *r*(t) being the reference output.

$$\begin{cases} e_1 = x_1 - r \\ e_2 = \dot{e}_1 = \dot{x}_1 - \dot{r} \\ \vdots \\ e_n = \dot{e}_{n-1} \end{cases} \tag{20}$$

and $\beta_i \ (i = 1, \cdots, n)$ is designed so that the polynomial $p^n + \beta_n p^{n-1} + \cdots + \beta_2 p + \beta_1$ is Hurwitz, and $\alpha_i \ (i = 1, \cdots, n)$ is designed as,

$$\begin{cases} \alpha_1 = \alpha, & n = 1 \\ \alpha_{i-1} = \frac{\alpha_i \alpha_{i+1}}{2\alpha_{i+1} - \alpha_i}, & i = 2, \cdots, n \ \ \forall n > 2 \end{cases} \tag{21}$$

with $\alpha_{n+1} = 1, \alpha_n = \alpha, \alpha \in (1 - \varepsilon, 1), \varepsilon \in (0, 1)$.

When the system state is driven onto the FOTSM defined as in the above, $s = 0$ is reached

and e_i $(i = 1, \cdots, n)$ in (19) will converge to the terminal sliding surface, and further converges to zero along the sliding surface within finite time. To achieve the convergence of system state in (18) in finite time, a full-order terminal sliding mode control scheme was proposed in [35]. However, this scheme requires known values of upper bound for $f(x)$ and $\dot{f}(x)$, which may not be available for some practical applications.

In this paper, we develop a new method that uses on-line estimation of the fault change rate by an adaptive RBF network, and combined with a FOTSM to drive the states onto the sliding surface. Thanks to using the RBF estimator, the upper bounds of fault and fault derivative originally required in [35] will not be required in this method.

In this new development, the RBF network, $NN(z): R^q \to R$, is defined as in (22) and is used to estimate the fault derivative, $\dot{f}(x)$ from the current system state as in (23).

$$NN(z) = \hat{W}^T \Phi(z) \tag{22}$$

$$\dot{f}(t) = NN(z) + \varepsilon \tag{23}$$

where ε is the approximation error, $z = [x_1, \cdots, x_n, \dot{x}_n] \in R^{n+1}$ is the input vector of the RBF network, $\Phi(z) = [\phi_1(z), \phi_2(z), \cdots, \phi_p(z)]^T \in \Re^p$ is the nonlinear basis function, $\hat{W} \in \Re^p$ is the weight vector. The Gaussian function is chosen in this research as the basis function,

$$\phi_i(z) = \exp(-\frac{\|z - c_i\|^2}{\sigma_i^2}), \quad i = 1, \cdots, p \tag{24}$$

where c_i the centre of the i^{th} hidden layer node and is a vector of the same dimension with z. σ_i is the radius of the i^{th} Gaussian function. We define an optimal weight W^* as in (25), which represents the optimal solution of weight W that gives the minimum approximation error ε^* in equation (23). There would exist such a W^* according to the universal approximation property of the RBF network.

$$\hat{W}^* = \arg \min_{\hat{W} \in \Omega_f} \left[\sup_{z \in S_z} \left| \hat{f}(z \mid \hat{W}) - f(z) \right| \right] \tag{25}$$

where $\Omega_f = \left\{ \hat{W} : \left\| \hat{W} \right\| \le M \right\}$ is a valid field of the estimated weight $\hat{W}$. $M > 0$ is a design parameter and $S_z \subset \Re^q$ is an allowable set of the NN input vectors. The optimal weight will then generate,

$$\dot{f}(z) = W^{*T} \Phi(z) + \varepsilon, \ \varepsilon \le \bar{\varepsilon} \tag{26}$$

where $\bar{\varepsilon}$ is a constant and the upper bound of the approximation error.

With the RBF network and the FOTSM manifold in (19), the control law in the developed method is designed with two parts.

$$u = b^{-1}(x)(u_1 + u_2) \tag{27}$$

$$u_1 = -g(x) - \beta_n e_n^{\alpha_n} - \cdots - \beta_1 e_1^{\alpha_1} + \ddot{r} \tag{28}$$

$$\dot{u}_2 = -\widehat{W}^T \Phi(z) - (k + \eta) sign(s) \tag{29}$$

where $k > \varepsilon_N,\ \eta > 0$ are two design parameters. The RBF estimator is adapted on-line with information provided by the states in the network input vector $z(x)$, and the adaptive law is designed as in (30).

$$\dot{\widehat{W}} = \frac{1}{\gamma} s\Phi(z) \tag{30}$$

with $\gamma > 0$ being the inverse of a learning rate. Given the designed control law and the adaptation law of the RBF network, the post-fault stability of the closed-loop system is established by the following theorem.

Theorem 1

In the nonlinear system presented by (18), if the full-order terminal sliding mode manifold is chosen as (19), and the control law and the network adaptation law are designed as in (27)-(30), then the state of the closed-loop system will converge to zero and system is stable.

Proof

The following Lyapunov function is used,

$$V = \frac{1}{2} s^2 + \frac{1}{2} \gamma_1 \widetilde{W}^T \widetilde{W}, \tag{31}$$

where $\widetilde{W} = W^* - \widehat{W}$ is the RBF network weight convergence error. Now, we derive the first-order derivative of V w.r.t. time as,

$$\dot{V} = s\dot{s} + \gamma_1 \widetilde{W}^T \dot{\widetilde{W}}. \tag{32}$$

Substituting (18) to (19) yields,

$$s = g(x) + f(x) - \ddot{r} + b(x)u + \beta_n e_n^{\alpha_n} + \cdots + \beta_1 e_1^{\alpha_1}. \tag{33}$$

The control u in (33) is replaced by the control law in (27) and (28),

$$s = f(x) + u_2. \tag{34}$$

Thus, we have

$$\dot{s} = NN(z) + \varepsilon + \dot{u}_2. \tag{35}$$

Then, substituting (23) and (29) into (35) yields

$$\begin{aligned} \dot{s} &= W^{*T} \Phi(z) + \varepsilon - \widehat{W}^T \Phi(z) - (k + \eta) sign(s) \\ &= \widetilde{W}^T \Phi(z) + \varepsilon - (k + \eta) sign(s). \end{aligned} \tag{36}$$

Substitute (36) and (30) into (32), we have

$$\dot{V} = s\widetilde{W}^T\Phi(z) + s\varepsilon - s(k+\eta)sign(s) + \gamma_1\widetilde{W}^T\dot{\widetilde{W}}$$
$$= \widetilde{W}^T\left[s\Phi(z) - \gamma_1\dot{\widehat{W}}\right] + s\varepsilon - (k+\eta)|s|$$
$$= s\varepsilon - (k+\eta)|s|$$
$$\leq (\varepsilon - k - \eta)|s|. \quad (37)$$

Here k, η are constants and to be selected in the design. We choose k, η such that $\eta > 0, k > \varepsilon_N \geq \varepsilon$, then, $(\varepsilon - k - \eta)|s| < 0$ for $s \neq 0$. This leads to $\dot{V} < 0$. According to the Lyapunov stability theorem, V will converge to zero. Thus, by the definition of V in (31) and the terminal sliding mode theorem [32], the system state is guaranteed to converge to zero on the sliding manifold in finite time, and the RBF network weights converge to the existing optimal weights.

□

Remark It is worth mentioning that the sign function is involved in $\dot{u}_2$ rather than in u_2, therefore the discontinuity caused by the sign function will not be used directly in the control law, but will be integrated. Thus, the control signal will be guaranteed continuous. Due to this technique, the chattering problem is eliminated and the developed method is made more acceptable by the industrial practitioners. Moreover, the singularity is avoided in the designed control as the derivative of s is not used.

The structure of the whole feedback system including the adaptive RBF estimator is displayed in Fig.2.

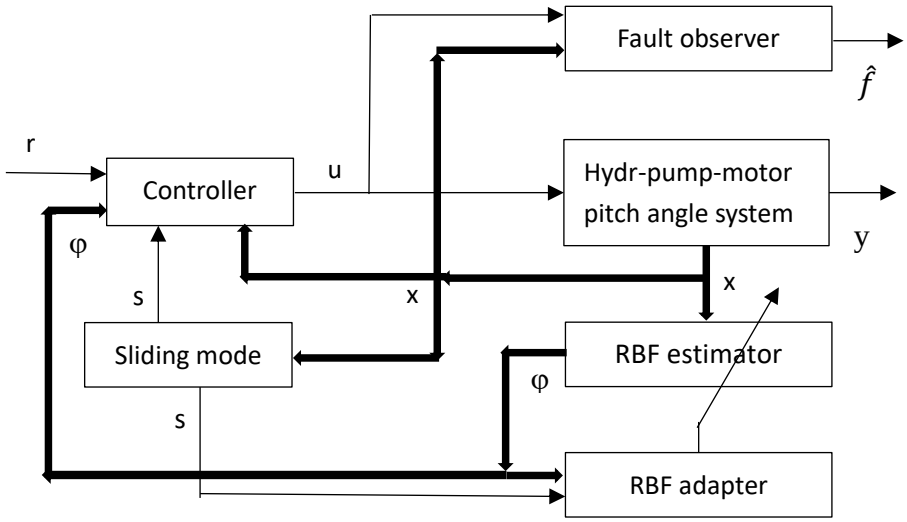

Fig.2 Schematic of fault tolerant tracking control of pitch angle

It is noticed that in active FDI methods, fault detection and fault tolerant control are designed separately, and the signals and information generated in fault detection are then used to help for fault tolerant control. In this paper, we detect the fault using the disturbance observer. If a fault is reported, we will schedule a repair and keep maintenance. At the same time, the designed fault tolerant control scheme maintains the system post-fault stability and keeps the

tracking control performance not degraded.

5. Simulation studies

The developed pitch angle tracking control with fault diagnosis and fault tolerance is evaluated using computer simulation. Two sets of desired pitch angles were used with one of step reference pitch angle and one of sinusoidal signal to represent abrupt and slow change of the wind speed. A step change of friction torque is simulated as an abrupt fault to be tested. The simulation is based on Matlab/Simulink, where the pitch angle drive plant and the disturbance observer are implemented in Simulink, while the adaptive RBF network and control algorithm are implemented with a Matlab-file. In each sample period, the Matlab-file calculates the control input, and then called the Simulink model to obtain the plant and fault observer outputs. The sample period in this research is 0.001 sec and the simulation runs for 8 sec. The detailed procedure is presented below.

Step 1 A Simulink model is established for the servo-hydraulic drive plant (equations (9)-(13)) and the disturbance observer ((14)-(17)). The Simulink model has two inputs: the friction change and control input; while has five outputs: system output of pitch angle, the other two states of motor shaft rotary speed and rotary acceleration, fault to be detected and the estimated fault. The values of the physical parameters in the hydraulic drive are given in Table 1.

Step 2 A Matlab file is coded to calculate the sliding surface according to (19)-(21), control variable according to (27)-(29), and neural estimator output according to (22)-(24) and weight updating according to (30).

Step 3 Simulate faults by changing the viscous frictional torque on motor axis, $T_p(t)$ as below to mimic the friction change.

Without fault: $T_p(t) = -40Nm$, for $0.6 < t < 1.4sec,\ 2.6 < t < 3.4sec,$
$4.6 < t < 5.4sec,\ 6.6 < t < 7.4sec.$

With fault: $T_p(t) = -160Nm$, for the rest of time in $0 < t < 8sec.$

Step 4 Design the sliding surface in this application, $n = 3$, so the sliding manifold in (19) is generated with $\alpha_1 = 0.3000, \alpha_2 = 0.3913, \alpha_3 = 0.5625, \alpha_4 = 1$ to satisfy (20) and $\beta_1 = 32.77, \beta_2 = 30.72, \beta_3 = 9.6,$ to set the three poles at $p_{1,2,3} = -3.2$, so that $p^3 + \beta_3 p^2 + \beta_2 p + \beta_1$ is Hurwitz.

Step 5 Design the RBF network with the centre, $c = [c_1, \cdots, c_{10}] = \begin{bmatrix} 0.1 & 0.2 & \cdots & 1.0 \\ 0.05 & 0.15 & \cdots & 0.95 \\ 0.0 & 0.1 & \cdots & 0.9 \\ 0.15 & 0.25 & \cdots & 1.05 \end{bmatrix}$,
width, $\sigma = [\sigma_1, \cdots, \sigma_{10}] = [0.5, 0.5, \cdots, 0.5]$, and initial value of the weight $W = [1,\ \ 1,\ \cdots, 1]^T * 10^{-5}$.

Step 6 Design the control $u(t)$ according to (27), where $u_1(t)$ from (28) and $u_2(t)$ from integration of (29). The control parameters in (37) are chosen as $k = 5, \eta = 2.$

Step 7 Design the adaptation law of the neural network estimator with equation (30), where the learning rate is chosen as $\gamma = 5.$

Four sets of simulations are conducted with different types of reference signals and different types of fault signals. The first one uses a square wave of reference pitch angle and the second one uses a sinusoidal reference pitch angle. The fault signal used in the first two simulations is square wave to mimic the abrupt fault. The third and fourth simulations use the same reference signal as the first two ones but sinusoidal fault signal to mimic the slowly developing fault.

The simulation results for the first set are displayed in Fig.3, where the reference pitch angle together with the controlled pitch angle are displayed in the middle figure for comparison. The top figure displays the sliding mode *s* and the bottom figure displays the real fault and the estimated fault by the designed disturbance observer. It can be seen in Fig.3 that the sliding mode is forced to approach zero from the nonzero initial value. When the fault occurs, the sliding mode, *s* just deviates away from zero, and is then maintained at zero for the whole simulation period. Then, in the middle figure, the first state i.e. the pitch angle converges to the reference output even when the fault occurs as shown in bottom figure in Fig.3. This demonstrates that the major objective, the fault tolerant tracking control is achieved successfully.

In the bottom figure in Fig.3 we can see that the estimated fault very closely follows the real fault occurred in the system, indicating that the estimated fault not only can detect fault by reporting fault occurrence, can also be used to report fault size and occurrence time. Although the specified fault has already been tolerant in the performance of pitch angle tracking, the fault diagnosis function will be used to inform the operator to schedule the detailed inspection and maintenance.

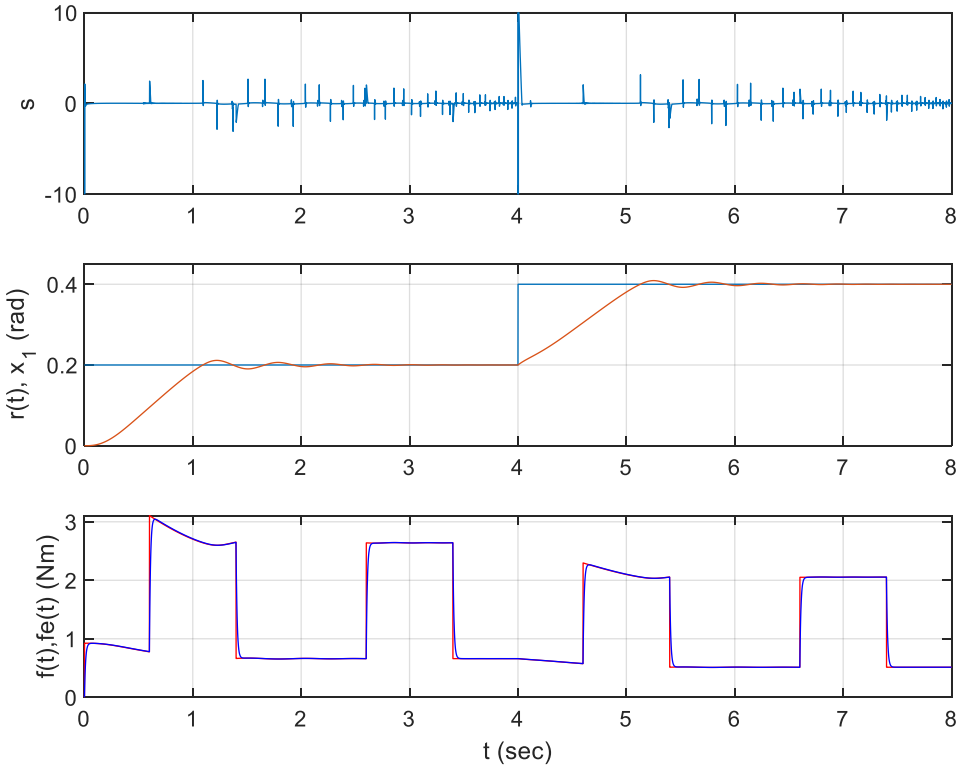

Fig.3 Performance of the pitch angle control system with step reference and fault
Top: sliding surface, middle: reference and actual pitch angles, bottom: actual and the estimated fault.

In Fig.4 the second state i.e. the rotary speed on hydraulic motor axis and the third state i.e. the rotary acceleration are displayed in the top and middle figures. We can see that both states are bounded on the effect of adaptive RBF network estimator, which is guaranteed by the employed Lyapunov theory in the derivation of the control law and the network weight updating law. The control variable is displayed in the bottom figure. We can see there is no chattering on the control, which guarantees the quality of the control system design, and this is due to the advanced feature of the full-order terminal sliding control strategy.

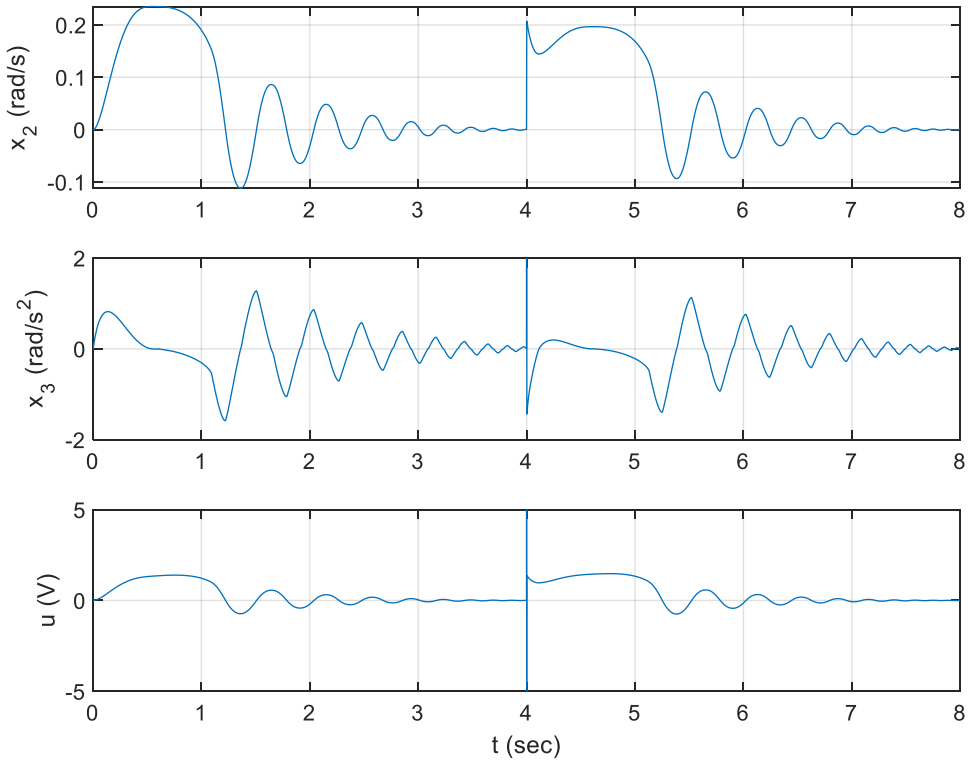

Fig.4 Performance of the pitch angle control system with step reference and fault
Top: second state or rotary speed of motor axis, middle: third state or rotary acceleration, bottom: control variable, the servo motor input.

In the second simulation, the reference pitch angle uses a sinusoidal signal, to evaluate the performance of the designed control system in tracking a time-varying reference. It is evident in Fig.5 that the sliding surface quickly converges to zero and maintained within a small region around zero. As the sliding surface is designed to include pitch angle tracking error and the error change rate, the convergence of the sliding mode will guarantee the tracking error converges to zero. The fault estimation also works when the reference signal is a time varying signal, which guarantees the detection of the fault. The pitch angle tracking was not affected by the simulated fault under the designed sliding mode control.

Fig.6 demonstrates that the second and third states are bounded in the whole simulation period for the time varying reference. Usually, closed-loop system stability is not too difficult to achieve without system fault. However, a system fault will change system dynamics so that the system stability is difficult to maintain after a fault occurs, especially for a severe nonlinear system. In this research, the RBF network is used to estimate and compensate for the change rate of the fault in on-line mode, so that the system stability is maintained. The bottom figure in Fig.6 indicates that there is no chattering in the control variable, and this is due to the full-order terminal sliding mode control scheme.

The third and fourth simulations use sinusoidal fault signal and remain the same reference pitch angle signal as in the first two simulations, and achieved very similar results as that in the first two simulations, the results are therefore not displayed for simplicity.

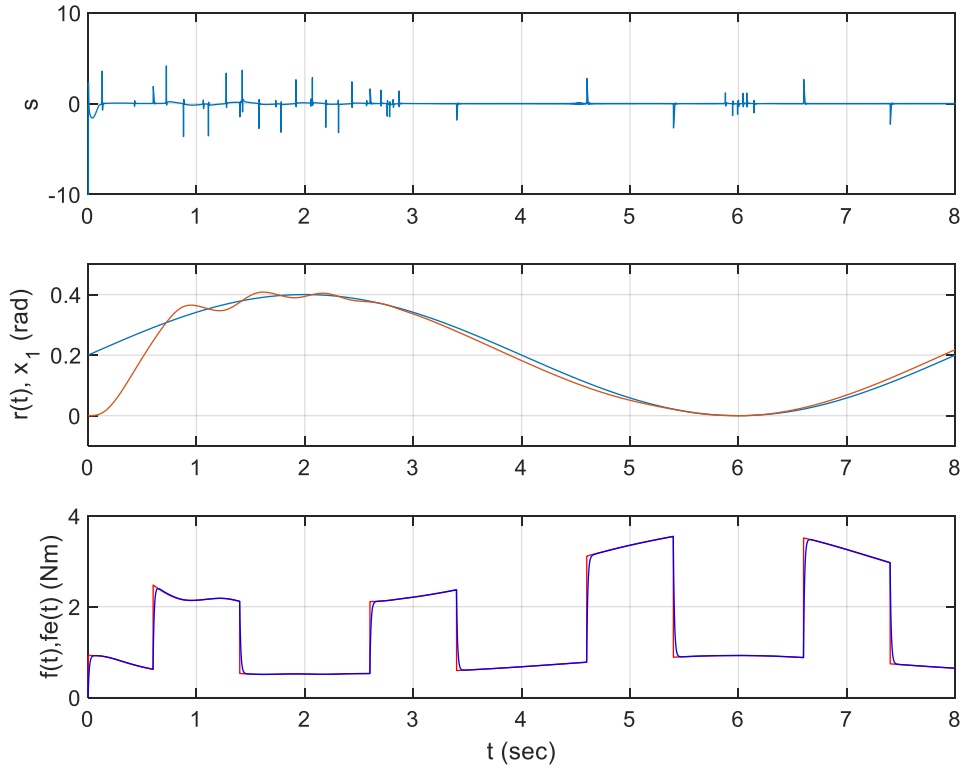

Fig.5 Performance of the pitch angle tracking control system with sinusoidal reference
Top: sliding surface, middle: reference and actual pitch angle, bottom: actual and the estimated fault.

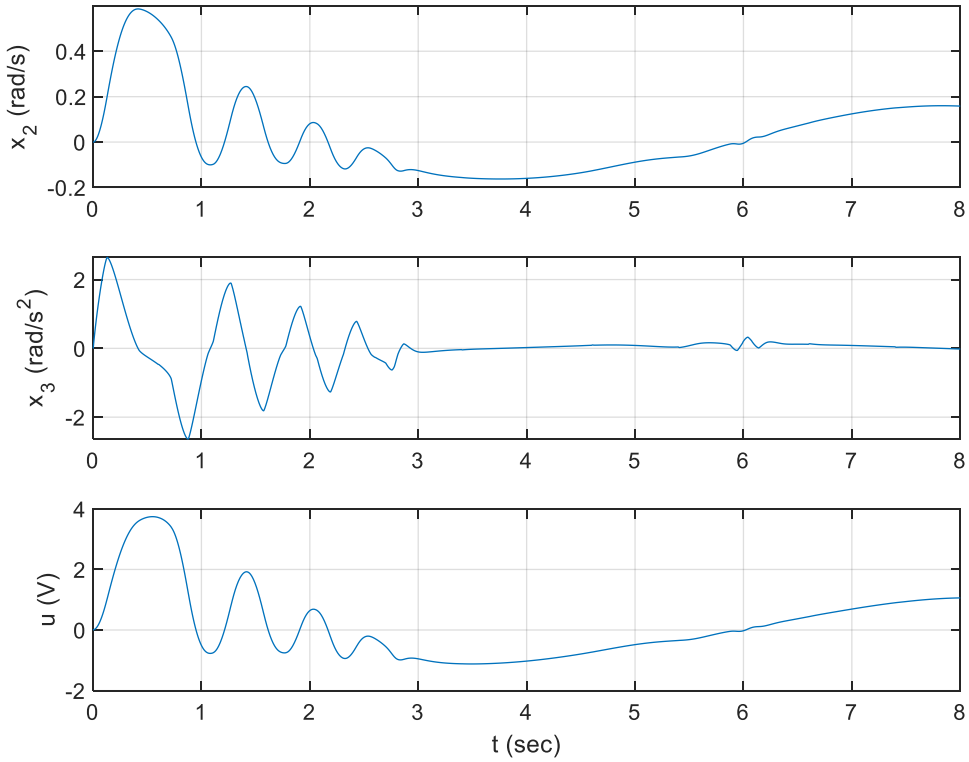

Fig.6 Performance of the pitch angle tracking control system with sinusoidal reference

Top: second state or rotary speed of motor axis, middle: third state or rotary acceleration, bottom: control variable, the servo motor input.

Similar simulations as described above have also been conducted where the fault is simulated with a sinusoidal signal to mimic a slowly developing fault. The simulations shown the similar results with pitch angle tracking, second and third states bounded, estimated fault follows real fault, control signal without chattering. These simulation results are therefore not displayed for simplicity.

6. Comparison studies

To demonstrate the superiority of the proposed fault tolerant control method over existing methods, we use a full-order terminal sliding mode control method without compensation developed in [35] as an example and do a comparison study. The method has a limitation to the amplitude of both disturbance and the change rate of disturbance, so that the robustness of the performance of the method is affected by the limitations.

For the system defined in (9)-(13) as copied below,

$$\dot{x}_1 = x_2$$

$$\dot{x}_2 = x_3$$

$$\dot{x}_3 = g(x) + b(x)u(t) + f(t)$$

The FOTSMC without compensation utilized a sliding manifold as below.

$$s = \dot{x}_n + \beta_n sign(x_n)|x_n|^{\alpha_n} + \cdots + \beta_1 sign(x_1)|x_1|^{\alpha_1}$$

where x_i $(i = 1, \cdots, n)$ is the system states and β_i $(i = 1, \cdots, n)$ is designed so that the polynomial $p^n + \beta_n p^{n-1} + \cdots + \beta_2 p + \beta_1$ is Hurwitz, and α_i $(i = 1, \cdots, n)$ is designed according to (21). The control law is designed as below.

$$u = b^{-1}(x)(u_1 + u_2)$$

$$u_1 = -g(x) - \beta_n sign(x_n)|x_n|^{\alpha_n} - \cdots - \beta_1 sign(x_1)|x_1|^{\alpha_1}$$

$$\dot{u}_2 + Tu_2 = -(Tk_d + k_{dd} + \varepsilon)sgn(s)$$

where k_d is the bound of the disturbance, k_{dd} is the bound of the change rate of the disturbance, and ε is a positive constant. Here both k_d and k_{dd} are supposed to be known.

The pitch angle control system with the model derived in the first part of the paper (9)-(13) is controlled using the above reviewed FOTSMC without compensation method for comparison. The same fault as defined in Step 3 of last Section and as depicted in Fig.3 is applied to the system for this simulation. Though the amplitude of the fault can be estimated, the change rate of the fault signal is difficult to predict. We used the following design parameters: $T = 0.1, k_d = 15, k_{dd} = 20, \varepsilon = 1$, β_i $(i = 1, \cdots, n)$ and α_i $(i = 1, \cdots, n)$are chosen the same as that used in Step 4 of the last Section. Using the same Simulink model of the system and re-coded M-file to implement the control, the simulation result is shown in Fig.7.

As can be seen in the top figure of Fig.7, states do not converge to the sliding manifold s=0, due to the fault signal. The sliding manifold tends to converge for small fault signal, and diverges when the fault signal jumps. The system state or output is correspondingly diverged with the sliding manifold as shown in the middle figure. Note that in the existing FOTSMC without compensation method tracking control is not used, and the state is supposed to converge to zero with a zero set-point. If a very big value of $k_{dd}$is used to cover the change rate of fault signal, this would cause a big neighbourhood area in which the control signal and consequently the state would exhibit chattering. Compare with the existing method, the proposed method in this paper utilized an adaptive neural network to estimate the fault, and made the state insensitive to the fault. More importantly, the developed adaptive neural network is involved in the Lyapunov method to derive the adaptation law and control law, so that the post-fault dynamics of the entire system is guaranteed stable.

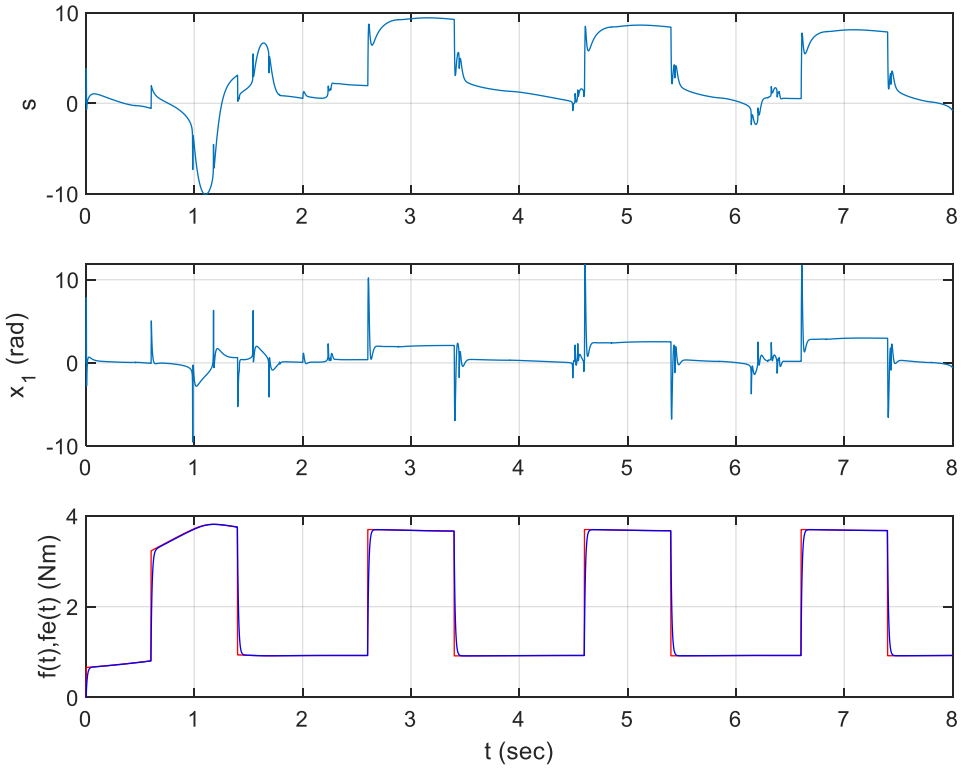

Fig.7 Response of full-order terminal sliding mode control

7. Conclusions

A fault tolerant tracking control system is designed in this paper with the FOTSMC and adaptive RBF estimator, and applied to pitch angle tracking control of wind turbine generation systems against the system fault of friction torque change. Also, a disturbance observer is designed to diagnose the occurred fault for the purpose of reporting fault occurrence, estimate fault size and the occurrence time. Combining the FOTSMC with the RBF estimator relaxes the limitation that requiring known bound of fault change rate. The designed system stability and the adaptive network convergence are guaranteed under the post-fault dynamics by using the Lyapunov method. The tracking performance was also maintained. The developed method is applied to variable-speed wind turbine generation systems to control the pitch angle. A servomotor-driven hydraulic pump-motor drive system is modelled with simulated fault injected. Simulation under Matlab/Simulink environment has been conducted to evaluate the effectiveness of the designed system. Simulation results show that the actual pitch angle tracks the squares and sinusoidal reference and tolerance with the fault occurrence. It suggests that the developed method has potential to be applied in industries to enhance reliability of engineering systems.

The further work of this research is to establish a hydraulic pitch system test rig with all sensors and actuators equipped. Then, real experiments can be attempted on the test rig to evaluate the reliability and performance of the developed fault tolerant control system. The

challenges would be the sensitivity of the developed algorithm to other non-pre-considered faults and signal-to-noise ratio may need to be adjusted.

Conflict of Interest: The authors declare that they have no conflict of interest.

References

[1] X. Yin, W. Zhang, X. Zhao, Current status and future prospects of continuously variable speed wind turbines: A systematic review, *Mechanical Systems and Signal Processing*, Vol.120, pp. 326-340, April 2019.

[2] Berrada, Y. and Boumhidi, I., New structure of sliding mode control for variable speed wind turbine, *IFAC Journal of Systems and Control*, Vol.14, December 2020, 100113.

[3] P. Li, W. Hu, R. Hu, Z. Chen, Imbalance fault detection based on the integrated analysis strategy for variable-speed wind turbines, *International Journal of Electrical Power & Energy Systems*, Vol.116, 105570, March 2020.

[4] O. Barambones, J.A. Cortajarena, I. Calvo, A. Karami-Mollaee, Variable speed wind turbine control scheme using a robust wind torque estimation, *Renewable Energy*, Vol.133, pp. 354-366, April 2019.

[5] Asgharnia, A., Jamali, A., Shahnazi, R., Maheri, A., Load mitigation of a class of 5-MW wind turbine with RBF neural network based fractional-order PID controller, *ISA Transactions*, Vol.96, pp. 272-286, 2019.

[6] Civelek, Z., Lüy, M., Çam, E., Barışçı, N., Control of pitch angle of wind turbine by fuzzy PID controller. *Intelligent Automation & Soft Computing*, Vol.22, Iss.3, pp. 463-471, 2016.

[7] Mahmoud, M.S., Oyedeji, M.O., Adaptive and predictive control strategies for wind turbine systems: A survey, *IEEE/CAA Journal of Automation Sinica*, Vol.6, Iss.2, pp. 364-378, 2019.

[8] Boukhezzar, B., Lupu, L., Siguerdidjane, H., Hand, M., Multivariable control strategy for variable speed variable pitch wind turbines, *Renewable Energy*, Vol.32, Iss.8, pp.1273-1287, 2007.

[9] Duong, M.Q., Grimaccia, F., Leva, S., Mussetta, M., Ogliari, E., Pitch angle control using hybrid controller for all operating regions of SCIG wind turbine system, *Renewable Energy*, Vol.70, pp.197-203, 2014.

[10] M.H. Chiang, A novel pitch control system for a wind turbine driven by a variable-speed pump-controlled hydraulic servo system, *Mechatronics*, Vol.21, Iss.4, pp. 753-761, 2011.

[11] M.A. Chowdhury, N. Hosseinzadeh, W.X. Shen, Smoothing wind power fluctuations by fuzzy logic pitch angle controller, *Renewable Energy*, Vol.38, pp. 224-233, 2012.

[12] T.L. Van, T.H. Nguyen, D.C. Lee, Advanced pitch angle control based on fuzzy logic for variable speed wind turbine systems, *IEEE Trans. on Energy Conversion*, Vol.30, Iss.2, pp. 578-587, 2015.

[13] I. Poultangari, R. Shahnazi, M. Sheikhan, RBF neural network based PI pitch controller for a class of 5-MW wind turbines using particle swarm optimization algorithm, *ISA Transactions*, Vol.51, Iss.5, pp. 641-648, 2012.

[14] H. Jafarnejadsani, J. Pieper, J. Ehlers, Adaptive control of a variable-speed variable-pitch wind turbine using radial basis function neural network, *IEEE Trans. Control Systems Technology*, Vol.21, Iss.6, pp. 2264-2272, 2013.
[15] W.M. Lin, C.M. Hong, T.C. Ou, Hybrid intelligent control of PMSG wind generation system using pitch angle control with RBFN, *Energy Conversion Management*, Vol.52, Iss.2, pp. 1244-1251, 2011.
[16] C.Y. Tang, Y. Guo, J.N. Jiang, Nonlinear dual-mode control of variable speed wind turbines with doubly fed induction generators, *IEEE Trans. on Control Systems Technology*, Vol.19, Iss.4, pp. 744-756, 2011.
[17] Y. Ren, L, Li, J. Brindley, Nonlinear PI control for variable pitch wind turbine, *Control Engineering Practice*, Vol.50, pp. 84-94, 2016.
[18] Geng, H., Yang, G., Output power control for variable-speed variable-pitch wind generation systems. *IEEE Trans. on Energy Conversion*, Vol.25, Iss.2, pp. 494–503, 2010.
[19] Colombo, L., Corradini, M., Ippoliti, G., Orlando, G., Pitch angle control of a wind turbine operating above the rated wind speed: A sliding mode control approach. *ISA Transactions*, Vol.96, pp. 95-102, 2020.
[20] Belghazi, O., Douiri, R., Cherkaoui, M., Power control of a wind energy based on a DFIG by sliding mode approach and pitch angle optimal control by genetic algorithm, *Journal of Achievements in Materials and Manufacturing Engineering*, Vol.74, Iss.2, pp. 78–85, 2016.
[21] Zribi, M., Alrifai, M., Rayan, M., Sliding mode control of a variable-speed wind energy conversion system using a squirrel cage induction generator, *Energies*, Vol.10, Iss.5, pp. 604, 2017.
[22] M. Chen, P. Shi, C.C. Lim, Adaptive neural fault tolerant control of a 3-DOF model helicopter system, *IEEE Trans. on System Man and Cybernetics: Systems*, Vol.46, Iss.2, pp. 260–270, 2016.
[23] C. Kwan, L.F. Lewis, Robust back-stepping control of nonlinear systems using neural networks, *IEEE Trans. on System Man and Cybernetics: Systems*, Vol.30, pp. 753–766, 2000.
[24] M. Van, M. Mavrovouniotis, S.S. Ge, An adaptive back-stepping non-singular fast terminal sliding mode control for robust fault tolerant control of robot manipulators, *IEEE Trans. on Systems, Man, and Cybernetics: Systems*, Vol.99, pp. 1-11, 2018.
[25] A.B. Trunov and M.M. Polycarpou, Robust fault diagnosis of state and sensor faults in nonlinear multivariable systems, *Proc. of the American Control Conference*, San Diego, California, June 1999.
[26] M.M. Polycarpou, A.B. Trunov, Learning approach to nonlinear fault diagnosis: detectability analysis, *IEEE Trans. on Automatic Control*, vol.45, Iss.4, pp. 806-812, 2000.
[27] S.W. Wang, D.L. Yu, Adaptive RBF network for parameter estimation and stable air–fuel ratio control, *Neural Networks*, Vol.21, Iss.1, pp. 102-112, 2008.
[28] S.W. Wang, D.L. Yu, A new development of IC engine air fuel ratio control, *ASME Journal of Dynamic Systems, Measurement and Control*, Vol.129, Iss.6, pp. 757-766, 2007.

[29] M. Xie, S. Yu, H. Lin, J. Ma, H, Wu, Improved Sliding Mode Control With Time Delay Estimation for Motion Tracking of Cell Puncture Mechanism, *IEEE Trans. Circuits and Systems*, Vol.67, Iss.9, pp. 3199-3210, April 2020.

[30] S. Li, H. Du, X. Yu, Discrete-time terminal sliding mode control systems based on Euler's discretization, *IEEE Trans. on Automatic Control*, Vol.59, No.2, pp. 546-552, 2014.

[31] L. Zhao, Y. Jia, Finite-time attitude tracking control for a rigid spacecraft using time-varying terminal sliding mode techniques, *Int. Journal of Control*, Vol.88, Iss.6, pp. 1150-1162, 2015.

[32] M. Jin, J. Lee, K.K. Ahn, Continuous non-singular terminal sliding mode control of shape memory alloy actuators using time-delay estimation, *IEEE/ASME Trans. on Mechatronics*, Vol.20, Iss.2, pp. 899-909, 2015.

[33] Y. Feng, X. Yu, Z. Man, Non-singular terminal sliding mode control of rigid manipulators, *Automatica*, Vol.38, Iss.2, pp. 2159-2167, 2002.

[34] J. Yang, S. Li, X. Yu, Sliding mode control for systems with mismatched uncertainties via a disturbance observer, *IEEE Trans. on Industrial Electronics*, Vol.60, Iss.1, pp. 160-169, 2013.

[35] Y. Feng, F. Han, X. Yu, Chattering free full-order sliding mode control, *Automatica*, Vol.50, Iss.4, pp. 1310-1314, 2014.

[36] X. Yin, W. Zhang, Z. Jiang, L. Pan, Adaptive robust integral sliding mode pitch angle control of an electro-hydraulic servo pitch system for wind turbine, *Mechanical Systems and Signal Processing*, Vol.133, 2019.